

# How supernova feedback turns dark matter cusps into cores

Andrew Pontzen<sup>1,2,3\*</sup>, Fabio Governato<sup>4</sup>

<sup>1</sup>Kavli Institute for Cosmology and Institute of Astronomy, Madingley Road, Cambridge CB3 0HA, UK

<sup>2</sup>Emmanuel College, St Andrew's Street, Cambridge, CB2 3AP UK

<sup>3</sup>Oxford Astrophysics, Denys Wilkinson Building, Keble Road, Oxford OX1 3RH, UK

<sup>4</sup>Astronomy Department, University of Washington, Seattle, WA 98195, USA

Accepted —. Received —; in original form —

## ABSTRACT

We propose and successfully test against new cosmological simulations a novel analytical description of the physical processes associated with the origin of cored dark matter density profiles. In the simulations, the potential in the central kiloparsec changes on sub-dynamical timescales over the redshift interval  $4 > z > 2$  as repeated, energetic feedback generates large underdense bubbles of expanding gas from centrally-concentrated bursts of star formation. The model demonstrates how fluctuations in the central potential irreversibly transfer energy into collisionless particles, thus generating a dark matter core. A supply of gas undergoing collapse and rapid expansion is therefore the essential ingredient. The framework, based on a novel impulsive approximation, breaks with the reliance on adiabatic approximations which are inappropriate in the rapidly-changing limit. It shows that both outflows and galactic fountains can give rise to cusp-flattening, even when only a few per cent of the baryons form stars. Dwarf galaxies maintain their core to the present time. The model suggests that constant density dark matter cores will be generated in systems of a wide mass range if central starbursts or AGN phases are sufficiently frequent and energetic.

## 1 INTRODUCTION

Over the last two decades, galaxies formed in numerical simulations based on the inflationary  $\Lambda$ CDM paradigm have suffered from a number of well-documented mismatches with observed systems. One of the most prominent of these has been the rotation curves of disk-dominated dwarf galaxies (e.g. Moore 1994; Flores & Primack 1994; for more recent updates see Simon et al. 2005, Oh et al. 2011b and references therein). The observed kinematics imply a constant density core of dark matter interior to 1 kpc, whereas simple physical arguments and simulations suggest that the cold dark matter density should be increasing roughly as  $\rho \propto r^{-1}$  to vastly smaller radii (e.g. Dubinski & Carlberg 1991; Navarro et al. 1996b).

Since some of the earliest work on dark matter profiles it has been suggested that sufficiently violent baryonic processes might be responsible for heating dark matter cusps into cores (Flores & Primack 1994). The proposed mechanisms identified in these papers fall in two broad categories: supernova-driven flattening (Navarro et al. 1996a; Gelato & Sommer-Larsen 1999; Binney et al. 2001; Gnedin & Zhao 2002; Mo & Mao 2004; Read & Gilmore 2005; Mashchenko et al. 2006, 2008), and dynamical friction from infalling baryonic clumps or disk instabilities (El-Zant et al. 2001; Weinberg & Katz 2002; Tonini et al. 2006; Romano-Díaz et al. 2008, 2009; Pasetto et al. 2010; Goerdt et al. 2010; Cole et al. 2011). Within the former category, most early works focused on a single, explosive mass-loss event. It then became clear that even with extreme parameters, such an event transferred insufficient energy to dark matter particles (Gnedin & Zhao 2002). On the other hand, Read & Gilmore (2005) showed that several more moderately violent bursts could be effective in creating a core. Increasingly sophisticated numerical work by Mashchenko et al. (2006,

2008) strongly supported the notion of stellar feedback and energy transfer from baryons to dark matter as the generator of cores, but did not fully explain the physical mechanism behind this transfer or follow the evolution of dwarf galaxies to  $z = 0$  to ensure that the cores were long-lived.

Recently, simulations were able to produce realistic, present-day cored dwarf galaxies within a fully cosmological context (Governato et al. 2010, henceforth G10). These simulations resolve individual star formation ‘clumps’ at the density of molecular clouds leading to galaxies that are additionally realistic because, like many observed dwarfs (Dutton 2009), they have no bulge – a consequence of preferentially expelling low-angular-momentum gas from the progenitors via naturally occurring galactic winds (Brook et al. 2011; see also Bullock et al. 2001 and van den Bosch et al. 2001). Oh et al. (2011a) confirmed that these effects bring the simulations into excellent agreement with observational constraints on stellar and HI content as well as those on overall mass distribution. By testing against dark-matter-only runs, G10 provided strong support to a model where the core flattening is generated by baryonic effects, in particular by rapid gas motions; moreover, a suite of comparison simulations revealed that these effects only become significant if stars form in dense clumps ( $\sim 100 \text{ amu cm}^{-3}$ ), suggesting that energy injection has to be concentrated in local patches (see also Ceverino & Klypin 2009).

The comparison of simulations with recent observations (Oh et al. 2011a) highlighted that feedback must occur in numerous relatively mild events to allow thin disks to form. However given the lack of analytic framework for understanding the microphysics of this process, the precise mechanism of supernova-driven cusp flat-

tening was not further elucidated in G10. Providing such a framework is the aim of the present work.

The remainder of this paper describes how to model the effects of small, central starbursts which create pockets of rapidly expanding gas and strong fluctuations in the local potential. Over time these repeated processes gradually transfer energy from the gas to the dark matter component. This has much in common with the view of Mashchenko et al. (2006, 2008) but places more emphasis on disrupting clumps as opposed to pushing them around, and clarifies that resonance<sup>1</sup> is not required. Because our picture can be modelled mathematically, we are able to validate it against the simulations, showing that the envisioned process indeed creates cores within the G10 simulations.

This paper is organized as follows. Section 2 introduces improved simulations based on those of G10, and discusses the characteristics of these simulations which predict cusp-flattening, thus motivating a study of orbits in rapidly changing potentials (Section 3). The initial discussion is, for simplicity, limited to power-law potentials but Section 4 removes this restriction, presenting more general equations to explain the detailed simulation results. We relate our work to the wider literature and conclude in Section 5, also discussing the realism of the underlying hydrodynamical evolution within the simulated galaxies. In a companion paper (Governato et al, in prep) we will discuss the scaling of the dark matter cores with galaxy masses.

## 2 THE SIMULATIONS

The smoothed particle hydrodynamics (SPH) simulations, run using the *Gasoline* code (Wadsley et al. 2004), are closely related to and improve upon those described in more detail by G10. The emphasis of the present work is on interpreting dynamical effects, rather than discussing the numerical methods in depth; however see Section 5 for brief comments on computational accuracy. Our new runs output more regular timesteps and include the effects of metal-line cooling according to the prescription of Shen et al. (2010). The simulations in this paper focus on the region hosting the galaxy denoted ‘DG1’ in G10. The ‘zoom’ technique (e.g. Katz & White 1993) allows for a high mass resolution of  $M_p = 3 \times 10^3 M_\odot$  (for gas particles) and  $M_p = 1.6 \times 10^4 M_\odot$  (dark matter) with a softening of 86 pc in a full  $\Lambda$ CDM cosmological context. We conducted analysis on the two most massive systems within this region: DG1 itself ( $M_{\text{vir}} = 3.7 \times 10^{10} M_\odot$  at  $z = 0$ ) and a somewhat smaller galaxy ( $M_{\text{vir}} = 1.3 \times 10^{10} M_\odot$  at  $z = 0$ ). Most results will be presented for the latter case, because the former undergoes a major merger at  $z = 3$ . Although our model does predict the correct flattening for DG1, its volatile merger history would introduce undue complexities into our discussion.

In the first run, denoted HT (“high threshold”), stars are allowed to form only at hydrogen densities exceeding  $100 \text{ cm}^{-3}$ . The second run, LT (“low threshold”), is identical to the first except that it allows stars to form at densities exceeding  $0.1 \text{ cm}^{-3}$ .

Adopting the higher threshold for star formation is strongly motivated by observational evidence that molecular clouds form at such densities (Bigiel et al. 2008; Tacconi et al. 2010). HT thus exhibits more realistic behaviour of the interstellar medium (e.g.

Saitoh et al. 2008). In particular, only at high formation thresholds exceeding  $\sim 10 \text{ cm}^{-3}$  will supernova feedback naturally give rise to bulk gas motions and outflows (Ceverino & Klypin 2009). This follows because individual high-density clumps are efficient in converting gas to stars, ultimately leading to vast overpressurization of the clump from the high local density of supernovae. The particular threshold value of  $100 \text{ cm}^{-3}$  for HT is chosen for consistency with G10, in which it was argued that this is the highest density which can be considered physical at our present resolution. We have also verified that when  $\text{H}_2$  physics is consistently included in simulations (Christensen et al, submitted; Governato et al, submitted) star formation indeed proceeds only at high densities even in the absence of an explicit threshold.

By contrast, LT’s threshold of  $0.1 \text{ cm}^{-3}$  represents an approximate historical norm for galaxy formation simulations (e.g. Navarro & White 1993; Katz et al. 1996) broadly compatible with the observed cut-off in star formation at low column densities averaged over  $\sim \text{kpc}$  scales (e.g. Kennicutt et al. 2007). Until recently LT would have been the most motivated choice; however, with the addition of metal-line cooling at increasing resolution we now prefer the HT simulations, using LT as a reference to understand why older simulations did not produce the effects of interest here.

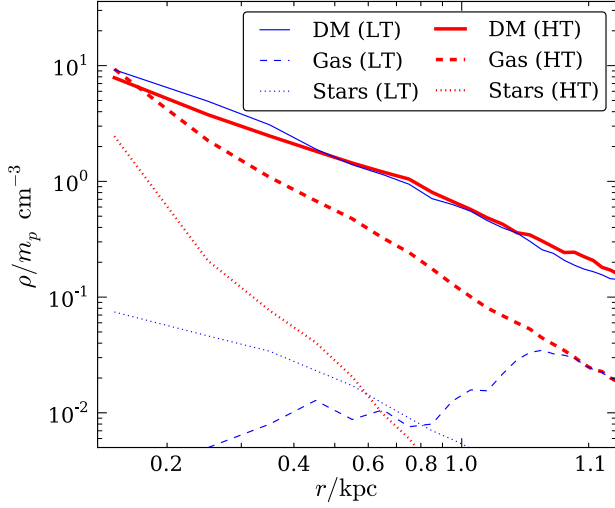
As expected following G10, LT remains cusped, unlike HT which develops a 1 kpc dark matter core at  $z = 0$  in both of its two most massive halos. In all cases the code consistently follows the feedback effects of the stellar populations (Stinson et al. 2006) so that, after a delay of  $\sim 10 \text{ Myr}$ , significant amounts of thermal energy are deposited into the surrounding gas. By  $z = 2$ , when HT has developed a stable core, LT and HT runs have formed an almost identical mass of stars ( $7 \times 10^7 M_\odot$ ) and therefore the same quantity of supernova energy has been released ( $7 \times 10^{56} \text{ ergs}$ ).<sup>2</sup> The failure of LT to lose its cusp thus reflects a difference in the coupling mechanism, not in the absolute energy deposition.

Figure 1 gives immediate insight into the difference between HT (cusp-flattening) and LT (cusp-preserving) simulations by showing their spherically-averaged halo density profiles shortly before the cusp begins to flatten in HT, at  $z = 4$ . Solid, dashed and dotted lines indicate respectively dark matter, gas and stellar density; thick red and thin blue lines represent the HT and LT runs in turn. In the LT run, the gas density cannot exceed the threshold of  $0.1 \text{ cm}^{-3}$ : stars are able to form and deposit supernova energy, preventing further cooling. In the HT run, by contrast, the gas density rises monotonically towards the centre because most of the gas is not eligible to form stars. The result is that the central gas density slightly exceeds that of the dark matter. It is natural to suppose from this that the halo will have a qualitatively different reaction to the presence of baryons in the two runs. (This work focuses on expansion of dark matter orbits, but we verified that the same processes operate on the similarly collisionless star particles in the simulation, the interesting implications of which are left for future study.)

Focusing on the HT simulation, Figure 2 (upper panel) shows the baryonic mass enclosed within 0.2, 0.5 and 1.0 kpc as a function of time. From around 1.7 Gyr after the big bang, the density near the centre undergoes order-of-magnitude fluctuations. First, gas flows in, cools and condenses near the centre of the potential well. Then, as the density of clumps rises above the  $100 \text{ cm}^{-3}$  threshold, star formation is allowed to proceed.

<sup>1</sup> Although Mashchenko et al. (2008) described their model as ‘resonant’, they have since stated that they did not mean to invoke a formal resonance, but rather the notion of changes in the potential occurring on roughly the dynamical timescale (Wadsley, pri. comm.).

<sup>2</sup> Note, however, that by  $z = 0$  the LT simulation forms  $4 \times 10^9 M_\odot$  in stars compared against the HT simulation’s  $5 \times 10^8 M_\odot$ . Only the HT simulation forms a realistic dwarf galaxy (Oh et al. 2011a).



**Figure 1.** Spherically averaged halo density profiles for high star-formation threshold (HT, thick red lines) and low threshold (LT, thin blue lines) simulations at  $z = 4$ , shortly before the dark matter profile starts to flatten in the high-threshold model. Solid, dashed and dotted lines show respectively dark matter, gas and stellar content. In the low threshold case, dark matter dominates by orders of magnitude at every radius. In the high threshold case, the gas reaches a comparable density to the collisionless matter in the central regions. Gaseous processes can therefore cause heating of collisionless components (dark matter and stars) in HT but not LT runs.

Once supernova energy is dumped into the gas, thermal expansion forms an underdense bubble of up to several kiloparsecs diameter (lower panel, Figure 2). The energy is initially deposited within a small volume (a consequence of the high star formation threshold) which then reaches temperatures of  $\sim 10^8$  K. The gas is vastly overpressurized relative to its surroundings, so expands at close to the thermal velocity (typically reaching  $\sim 300$  km/s  $\simeq 0.3$  kpc/Myr). Compared to the orbital timescales, which are  $\gtrsim 25$  Myr, the bubble formation is effectively instantaneous.

The adiabatic cooling from the expansion is included, but the bubbles nonetheless remain hot ( $\sim 10^6$  K) by the time they reach rough pressure equilibrium with the remainder of the disk. They are then sufficiently underdense ( $\sim 10^{-2}$  cm $^{-3}$ ) that the radiative cooling timescale is up to 100 Myr; the bubble can therefore persist for this length of time, after which it cools back into the disk if it has not actually escaped in a galactic wind. The rapid, repeated fluctuations in the central mass content of the simulated galaxy are similar to those shown in Figure 3 of Mashchenko et al. (2008). However we have verified that, in our case, this is due to the gas being heated and expanding outward rather than remaining in rapidly-moving coherent clumps as suggested by Mashchenko et al. (2008).

The overall picture for the dark matter is insensitive to the ultimate destination of the gas, requiring only the intermittent variations explained above; the present work makes no assumptions about mass loss. Note, however, that significant winds do exist in the simulations; the final baryon fraction in the galaxies is only 25% of the cosmic value (G10) and only 3% of the baryons have been turned into stars. The winds have been shown to be important in matching the star formation rates, distribution of stars and final baryon fractions of the dwarf galaxies (see McGaugh et al. 2010; Brook et al. 2011; Oh et al. 2011a).

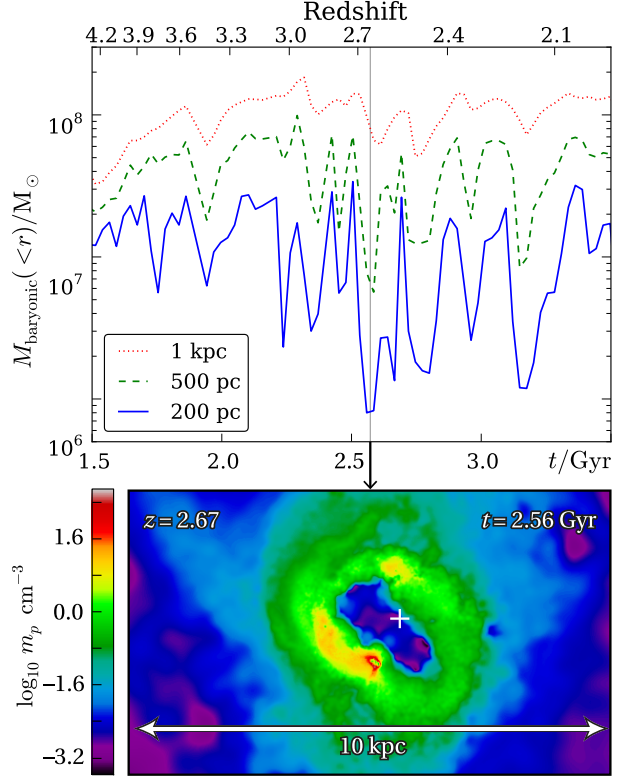


**Figure 2.** (Upper panel) The baryonic mass interior to, from top line to bottom, 1 kpc, 500 pc and 200 pc (HT simulation). Bursty central star formation coupled to strong supernova feedback causes coherent, rapid oscillations in the potential interior to 1 kpc. The orbital time of typical dark matter particles interior to 1 kpc is  $\gtrsim 25$  Myr. By contrast the simulated supernova bubbles can encompass the inner kiloparsec in around 3 Myr, far too rapidly for the adiabatic approximation to be valid. The lower panel shows the disk-plane density during the starburst event at  $t = 2.56$  Gyr,  $z = 2.67$ . A large underdense bubble has formed at the centre of the disk through thermal expansion of gas heated by multiple supernova explosions. The cross marks the halo centre.

### 3 ANALYTICAL MODEL

This Section discusses how the energy of a single dark matter particle (or star) changes in response to a fluctuating potential sourced by gas subject to processes described above. Two restrictions on the calculation are imposed throughout the paper:

- (i) the potential is assumed to be spherically symmetric;
- (ii) the tracer particles are assumed to be massless, *i.e.* the potential is always external.

The latter condition represents a decision to focus on the micro-physical mechanism via which particles gain energy, rather than the subsequent evolution of the self-gravitating system. The first condition could in future be relaxed, but makes calculations much simpler because particles orbit in the 1D effective potential

$$V_{\text{eff}}(r; j, t) = V(r; t) + \frac{j^2}{2r^2}, \quad (1)$$

where  $V(r; t)$  is the time-dependent physical potential and  $j$  is a conserved angular momentum.

For simplicity we will temporarily impose two further restrictions which will later be removed in Section 4:

- (iii) only the normalization of the potential changes, *i.e.* its functional form is fixed;
- (iv) the functional form of the potential is a power law.

Together these imply that the underlying potential in (1) is specified by  $V(r; t) = V_0(t)r^n$ . Some useful test cases fall into this exact form: a Keplerian orbit has  $n = -1$  while a harmonic oscillator implies  $n = 2$ . The final case will be of particular interest chiefly for its analytic simplicity, but we also note that it corresponds to assuming a spatially constant density of matter.

The rate of change of the total energy of a particle orbiting within the potential,  $dE/dt$ , is given by the partial derivative  $\partial V / \partial t|_{r(t)}$ , where  $r(t)$  denotes the solution to the equations of motion. In the limit of an instantaneous change in the potential  $V \rightarrow V + \Delta V$  occurring at time  $t$ , the total energy of the particle therefore changes by  $\Delta E = \Delta V(r(t)) = \Delta V_0 r(t)^n$ .

Assuming we have no prior knowledge of the phase of the particle, the virial theorem (e.g. Goldstein et al. 2002) states that the expected potential energy is

$$\langle V \rangle = \frac{2E_0}{2+n}, \quad (2)$$

where  $E_0$  is the total energy of the particle and the result is independent of  $j$ . This and following equations are also therefore valid in the one-dimensional ( $j = 0$ ) subcase.

If suddenly  $V_0 \rightarrow V_0 + \Delta V_0$ , the energy after the potential change is  $E_0 + \Delta E_1$ , where

$$\langle \Delta E_1 \rangle = \Delta V_0 \langle r^n \rangle = \frac{2E_0}{2+n} \frac{\Delta V_0}{V_0}. \quad (3)$$

The fiducial adiabatic limit can be attained from here by assuming  $\Delta V_0$  and  $\Delta E_1$  to be infinitesimal and integrating over a series of such changes taking  $V_0$  smoothly to  $V_f$ . This yields a final, finite change in energy:

$$E_{f,\text{adiabatic}} = E_0 \left( \frac{V_f}{V_0} \right)^{2/(2+n)}. \quad (4)$$

As expected in the adiabatic limit, equation (4) implies no energy shift, regardless of the intermediate states, if the final potential is the same as the initial. This is the central problem of the adiabatic approximation. Figure 2 shows that the final distribution of gas will indeed be very similar to the initial, and therefore that the adiabatic prediction will be for no change in the final distribution of dark matter.

However Section 2 showed that potential changes in the simulations take place on timescales much shorter than the dynamical time, because the expansion speeds of the supernova-induced bubbles are much larger than the local circular velocity. As the gas expands and leaves the galaxy centre, the potential undergoes a series of large, instantaneous jumps, invalidating the adiabatic result given by equation (4).

Instead of integrating, one should therefore recursively apply equation (3) to each finite change. If, for instance, the potential switches immediately back to its original depth, the second shift in energy is given by

$$\langle \Delta E_2 \rangle = \frac{2(E_0 + \langle \Delta E_1 \rangle)}{2+n} \frac{-\Delta V_0}{V_0 + \Delta V_0}, \quad (5)$$

where the angular brackets indicate averaging over the orbital phase of our chosen trajectory during both the initial and final instantaneous potential jumps. These conditions are justified because the initial blowout is not causally connected to the location of a single tracer particle, nor is the exact fractional number of orbits between

initial blowout and eventual recollapse predictable (this aperiodicity is illustrated by Figure 2). By Taylor expanding, we find that the expected final energy of the orbit is given by

$$\langle E_f \rangle = E_0 + \langle \Delta E_1 + \Delta E_2 \rangle \simeq E_0 + \left( \frac{\Delta V_0}{V_0} \right)^2 \frac{2n}{(2+n)^2} E_0, \quad (6)$$

which is always an energy gain for bound orbits since  $E_0 < 0$  for  $n < 0$ . The energy gain is second order in the potential change  $\Delta V_0$ , but linear in the energy. One may verify that, if the potentially first changes suddenly but then gradually (*i.e.* adiabatically) relaxes to its original state, we will also see an increase in expected final energy of the same magnitude. The essential point is for the initial change to be rapid; the energy shift will then follow.

The special case of the harmonic oscillator ( $n = 2$ ) is helpful in demonstrating the origin of this energy shift, because its dynamics are especially simple. The potential is separable in Cartesian coordinates which means that we can assume the one-dimensional subcase without loss of generality. Then, for the case of sudden discrete jumps, the analytic form of the solution is written

$$x(t) = A \cos(\omega t + \psi), \quad (7)$$

where  $\omega^2(t) = 2V_0(t)$  while  $A(t)$  and  $\psi(t)$  specify the amplitude and phase of the oscillation, which change discontinuously with the potential. The new values of  $A$  and  $\psi$  after any jump can be determined either through energy arguments as above or by requiring continuity of both  $x$  and  $\dot{x}$ . Without loss of generality, we let  $\omega$  change from  $\omega_0$  to  $\omega_1$  at  $t = 0$ . The amplitude of the trajectory after the jump,  $A_1$ , is given by the expression

$$A_1^2 = A_0^2 \left[ 1 + \frac{\omega_0^2 - \omega_1^2}{\omega_1^2} \sin^2 \psi_0 \right], \quad (8)$$

which is explicitly dependent on the orbital phase  $\psi_0$  at which the discontinuity occurs. The corresponding change of energy is

$$\Delta E_1 = -E_0 \frac{\omega_0^2 - \omega_1^2}{\omega_0^2} \sin^2 \psi_0. \quad (9)$$

We can now analyze the changes in a single trajectory which lead us to recover the expected gain in orbital energy under a single blowout-recollapse cycle, equation (6). Figure 3 (thick line) shows an example orbit for which  $\omega_0^2 = 10\omega_1^2$ . The initial amplitude is unity until, at a certain time, the potential flattens out as mass is lost from inside the orbit. Intuitively, or from equation (9), this must always involve a loss of energy for the particle (since  $\omega_0^2 > \omega_1^2$ ); see also panel 1 at the top of Figure 3. However, according to equation (8), the new potential is sufficiently flattened that the orbital amplitude is now larger than unity (panel 2). This is crucial because the energy gain made when the potential change is later reversed ( $\omega$  returns from  $\omega_1$  to  $\omega_0$ ) will be accordingly larger, scaling with  $\langle x^2 \rangle$  (panel 3). Applying equations (8) and (9) for the reverse jump (*i.e.* with  $\omega_1$  and  $\omega_0$  exchanged) allow this picture to be directly verified.

This makes more concrete the assertion of equation (6) that one always expects to gain energy during a series of potential changes. Yet seen from another perspective, such a claim still needs to be reconciled with the underlying dynamics which are fully time-reversible. For instance, the time-reverse of Figure 3 (viewing the figure from right to left) represents an equally valid trajectory of the forwards dynamics and yet *loses* energy.

Under time-reversal, the blowout phase maps onto the recollapse phase and vice-versa. The irreversibility thus arises not from dynamical differences but statistical differences between the

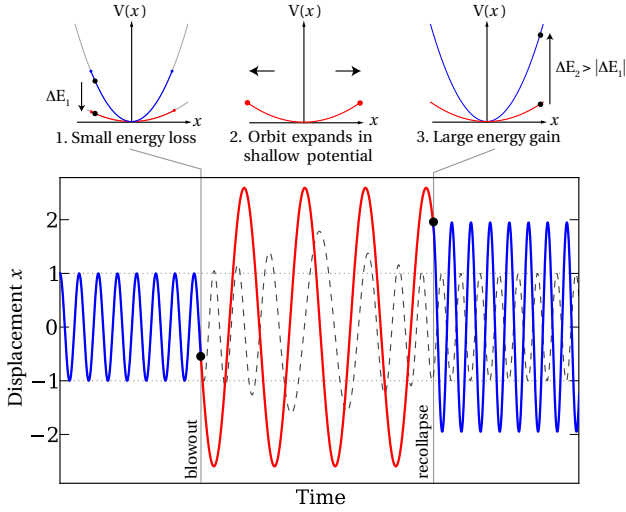


**Figure 3.** The mechanism for injecting energy into the dark matter orbits, illustrated by the exact solution for a time-varying harmonic oscillator potential. The lower panel shows (solid line) a solution to the equations of motion where  $\omega^2 = 1$  (blue) at early and late times, while at intermediate times  $\omega^2 = 0.1$  (red) mimicking baryonic blowout and recondensation. The changes in potential occur instantaneously; in this case the final amplitude of the oscillation is approximately twice that of the initial orbit. The dashed line shows the solution when the potential changes smoothly over several orbital periods; this gives adiabatic behaviour, so that the final orbit regains the initial amplitude, demonstrating the necessity for relatively sudden potential jumps. The inset figures (top) illustrate how the post-blowout orbit expansion implies that the late-time energy gain dominates over the initial energy loss.

forwards-blowout and reverse-recollapse pictures. In particular a uniform prior on the orbital phase before a transition is always assumed,  $2\pi p(\psi_0) = 1$ . On the other hand the phase  $\psi'_0$  after the transition is determined by

$$\tan \psi'_0 = \frac{\omega_0}{\omega_1} \tan \psi_0, \quad (10)$$

and, accordingly, the probability distribution function of  $\psi'_0$  is

$$2\pi p(\psi'_0) = \left( \frac{\omega_0}{\omega_1} \cos^2 \psi'_0 + \frac{\omega_1}{\omega_0} \sin^2 \psi'_0 \right)^{-1}. \quad (11)$$

The precise functional form (11) is not crucial, only that  $p(\psi'_0)$  cannot be taken to be uniform. After the sudden baryonic blowout, collisionless particles enter their new orbit in a special phase – preferentially near pericentre – so that they subsequently migrate outwards in unison.

It is this difference in knowledge of phases before and after sudden changes that allows irreversibility in the real universe to appear in the model. Only if all collisionless particles were near their pericentre just before the baryons returned would the statistical properties of the reversed picture match those of the actual model. While this is dynamically possible, it is statistically unlikely.

Finally note that if the changes in potential are introduced gradually, the process should become adiabatic and hence reversible. The dashed line in Figure 3 shows a numerical solution for which  $\omega$  changes smoothly over several orbital times from  $\omega_0$  to  $\omega_1$ , then back to  $\omega_0$ . As expected from equation (4), the final orbital amplitude is the same as its initial value, confirming the

qualitatively different results to be expected from gradual variation as opposed to sudden jumps.

#### 4 VALIDATING THE ANALYTIC MODEL AGAINST SIMULATIONS

To test the picture expounded above we start by generating a time-dependent effective toy potential from the simulations (Section 2). This is given by equation (1), with  $V(r;t)$  calculated from the spherically averaged density profile. The starting energy  $E_0$  and the value of  $j$  can be determined by specifying initial orbital parameters. The angular momentum is necessarily conserved because of the spherical symmetry of the modelling (restriction 1 of Section 3). In the simulations the changes in potential are not exactly symmetric (e.g. lower panel of Figure 2); however we will see below that, for the purposes of calculating real-space density profiles, the symmetric approximation which enforces constant  $j$  actually works extremely well.

As before, the energy shift for one jump is given by averaging over possible orbital phases. However the potential  $V_{\text{sphere}}$  is no longer an exact power law, so the calculation required is

$$\begin{aligned} \langle \Delta E \rangle &= \frac{\int \Delta V_{\text{eff}}(r(t)) dt}{\int dt} \\ &= \int \frac{\Delta V_{\text{eff}}(r) dr}{\sqrt{E - V_{\text{eff}}(r)}} \bigg/ \int \frac{dr}{\sqrt{E - V_{\text{eff}}(r)}}, \end{aligned} \quad (12)$$

where the time integrals are evaluated over an orbital period; after changing variables to  $r$  this corresponds to integrating over the region where the integrand is real. Equation (12) agrees with equation (3) for the special case of power-law potentials.

The remainder of this Section applies expression (12) recursively to a time-series of potentials from the HT (cusp-flattening) simulation, at each step updating  $\Delta V$ ,  $E$  and  $V_{\text{eff}}$  appropriately<sup>3</sup>. The energy gain is evaluated at every stored simulation timestep; the relevant outputs are written every  $\delta t \simeq 27 \text{ Myr}$ . Thus changes occurring on timescales  $\leq \delta t$  will implicitly be classified as “rapid” (composed of one jump) whereas those occurring on timescales  $\gg \delta t$  will automatically be treated as “adiabatic” (composed of many small steps). While the boundary between these limits cannot be uniquely defined, the change in behaviour must occur at around the orbital period for a particle, which is indeed  $\sim 25 \text{ Myr}$ . We verified by running checks with only every second timestep ( $\delta t \simeq 54 \text{ Myr}$ ) that the results presented are insensitive to the precise time-slicing.

The solid lines in Figure 4 show the resulting mean radius  $\langle r \rangle$  of orbits as a function of time, where

$$\langle r \rangle = \int \frac{r dr}{\sqrt{E(t) - V_{\text{eff}}(r; j, t)}} \bigg/ \int \frac{dr}{\sqrt{E(t) - V_{\text{eff}}(r; j, t)}}. \quad (13)$$

The values of  $j$  and  $E_0$  for each orbit are chosen by requiring the initial motion to be circular at a range of different radii. As time progresses, the orbits starting interior to  $1 \text{ kpc}$  migrate outwards, reflecting a net gain in energy. Orbits outside this radius are largely

<sup>3</sup> Because  $E$  takes a random walk, a more accurate result is in principle attainable by keeping track of its evolving distribution function rather than just its expected value. Our approach here is akin to taking the first term in a Fokker-Planck analysis and will be an excellent approximation because the energy shifts are approximately linear, as can be shown by generalizing equation (3).

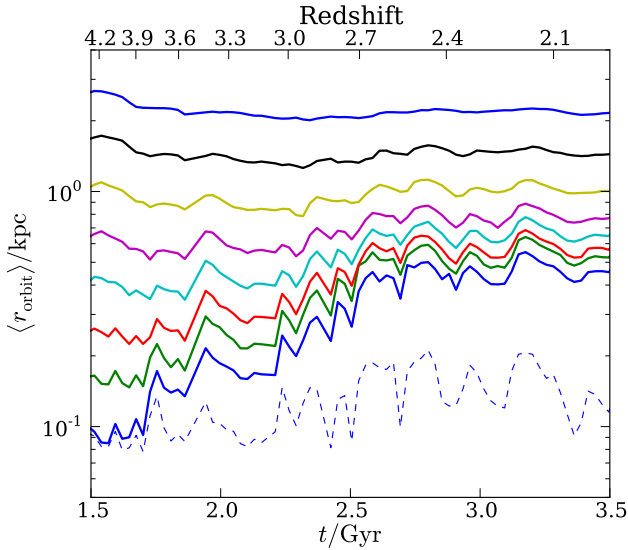


**Figure 4.** Using the spherically averaged potential from the simulations, we model the expansion of orbits of test particles at different initial radii (solid lines). Orbits starting significantly within the inner kiloparsec migrate outwards over several gigayears, whereas those starting outside a kiloparsec do not feel the rapid potential variations and so remain near their initial radius. Our model thus explains the flattening of central density cusps into kiloparsec-scale cores in small galaxies through radial outwards migration. As expected the reversible, adiabatic model (illustrated for the innermost orbit by the dashed line) does not correctly model the heating effect of very rapid potential variations in the inner parts of the halo.

unaffected. In the LT run, by contrast, no tracer particles gain energy; those that start on circular orbits, for instance, are predicted to remain at the same radius for the entire run.

Figure 2 implies that the central baryonic potential returns to its approximate original shape at the end of each starburst cycle, because the gas affected by the supernovae has cooled back into the disk (or has flowed out, replaced by fresh gas). In the adiabatic limit, where all potential changes occur slowly, the final orbital parameters should return to their initial values. Indeed by making  $\Delta V_{\text{eff}}$  infinitesimal and integrating (12) one obtains

$$\int \sqrt{E(t) - V_{\text{eff}}(r; j, t)} dr = \text{constant}, \quad (14)$$

where again the integral is taken over the real region of the integrand. This is the generalization of equation (4), and is exactly the adiabatic invariant derived through the action-angle approach (e.g. Binney & Tremaine 1987). It implies that  $E_{\text{final}} = E_{\text{initial}}$  if the potential returns to its initial form via a series of slow changes.

Demanding the adiabatic invariant (14) is constant yields the orbital migration in the ‘gradual outflows’ scenario. The dashed line in Figure 4 shows that the result derived in this limit is as expected: although temporary changes in the orbital radius do occur, they do not persist over time. This underlines the difference between our new model (where a tracer particle picks up energy from baryons) and the older adiabatic calculations (where the energy of a tracer particle is conserved).

Although Figure 4 shows that orbits gain energy, it cannot be used directly to infer the final inner profile of the dark matter. To draw conclusions about the evolution of the slope, we evolved the energy of  $\sim 90000$  orbits corresponding to all dark matter particles in the halo at  $z = 4$ . At each timestep, the full radial probability

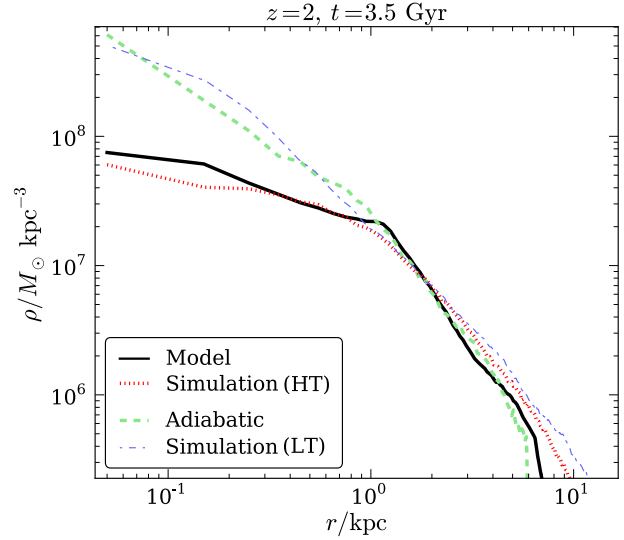


**Figure 5.** The spherically averaged dark matter density as a function of radius, measured at  $z = 2$  when the core has formed in the HT simulations (thick dotted line). The solid line shows the density profile at this time according to our model (see text for details); this is seen to be in excellent agreement with the HT simulation. The adiabatic model (dashed line) fails to correctly model the cusp flattening, demonstrating the need for the improved modelling presented here. The LT comparison simulation (dash-dotted line) also remains cusped as explained in Section 2.

distribution for each particle,

$$p(r; E, j) \propto \frac{1}{\sqrt{E - V_{\text{eff}}(r; j)}}, \quad (15)$$

was calculated numerically. The sum of the normalized probability distributions for all particles then implies a density profile according to

$$\rho_{\text{model}}(r) \propto \frac{1}{r^2} \sum_i p(r; E_i, j_i), \quad (16)$$

where the sum is over all tracer particles. Time evolution of  $\rho_{\text{model}}(r)$  arises from updating  $V_{\text{sphere}}$  and each  $E_i$  at every timestep according to equation (12); or, for comparison, by solving equation (14) to derive the behaviour in the adiabatic limit.

Starting at  $z = 4$ , the distribution function is evolved in this way to  $z = 2$ ; the resulting density profiles are illustrated in Figure 5. The thick solid line shows our main model [i.e. it is derived from equation (12)], and is seen to be in excellent agreement with the output of the simulation (dotted line). The dotted line shows the results of modelling the baryonic effects using the adiabatic approximation [i.e. equation (14)]; the cusp remains, contrary to the results of the simulation. This reaffirms that the adiabatic approximation does not capture important aspects of the impact of baryons on the dark matter. Finally, the dash-dotted line shows the profile from the LT (low star formation threshold) simulation which, as explained in Section 2, retains its cusp and is therefore in approximate agreement with the adiabatically evolved case.

The calculation described by equation (12) involves calculating the particle distribution function for every intermediate step. It is possible, therefore, to monitor the rate at which the cusp flattens and compare it against the simulations. Figure 6 shows the time evolution of the measured logarithmic slope at 500 pc for both the model density profile, equation (16), and the simulated density



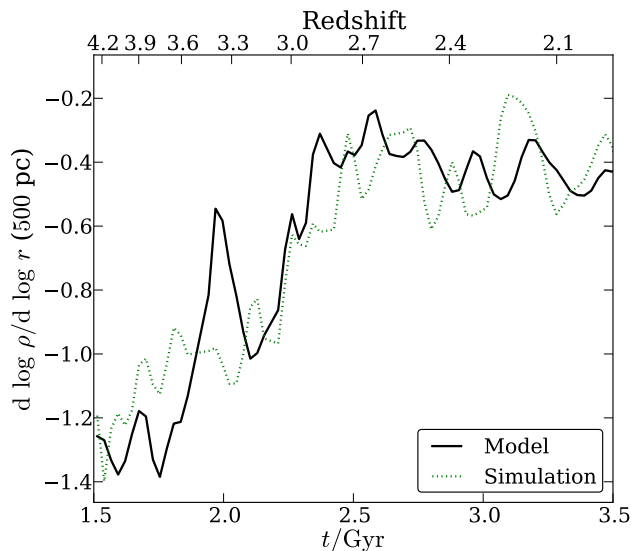


**Figure 6.** The evolution of the logarithmic slope of the halo in the raw simulation data (dotted line) and according to our model (solid line), measured at 500 pc in both cases. Values  $\lesssim -1$  indicate a conventional NFW-style cusp; shallower profiles are indicated by values closer to zero. The flattening of the profile in the simulations has previously been demonstrated to agree with observational data (Oh et al. 2011a). Our physical model for the origin of the flattening is in excellent agreement with the detailed simulation results.

profile. As time progresses, both the simulated and model density profiles gradually flatten out, with the value rising from  $< -1.0$  (cusped) to  $\sim -0.4$ , consistent with observations (Oh et al. 2011a).

To conclude, the analytic model presented here predicts flattening of the slope at the same rate as seen in the HT simulation (Figures 5 and 6); whereas the adiabatic approximation does not predict any significant flattening (Figure 5). We further verified that the new model did not predict a change in slope for the LT run in which the gas density remains too small to generate significant fluctuations in the potential. Overall, the new model alone provides a convincing explanation for the flattening processes seen by G10.

## 5 CONCLUSIONS

We have proposed a new analytic model that accounts for the flattening of dark matter cusps into cores. Energy is transferred into dark matter particle orbits through repeated, rapid oscillations of the central gravitational potential. These oscillations are caused by recurrent, concentrated bursts of star formation which induce rapid expansion of gas through supernova feedback heating. We verified that this process quantitatively accounts for cusp-flattening in a novel set of simulations similar to those in G10. The simulations include the effects of metal-line cooling, but like those in G10 form thin stellar disks and have a galactic star formation efficiency of only a few per cent. A comparison simulation (LT) with lower star formation density threshold does not form a core, despite forming ten times as many stars by  $z = 0$ . The model correctly predicts no cusp-flattening in this case (Figure 6) confirming our interpretation that for cores to form the supernova energy must be injected in a concentrated region (Figure 1).

The baryons do not have to escape the system completely, but only temporarily vacate the central regions, because the en-

ergy transfer is inherently irreversible. The G10 simulations do exhibit galactic-scale outflows which remove 75% of baryons by  $z = 0$ . These outflows have other important effects (e.g. Brook et al. 2011), yet the mass involved is only around a third of the mass involved in the central blowout-recollapse cycle. The relation between the galactic outflows and the local feedback will be the focus of future work.

The picture is related to the more established view that removal of baryons through galactic superwinds could cause the central dark matter profile to flatten (e.g. Navarro et al. 1996a; Gnedin & Zhao 2002; Read & Gilmore 2005). However, our model confirms that extreme, violent mass-loss events are not necessary, as suggested by (Mashchenko et al. 2006, 2008). This is important because the more moderate heating events allow retention of baryons and the formation of a thin stellar disk.

Dynamical friction from infalling baryonic clumps (El-Zant et al. 2001; Mo & Mao 2004; Romano-Díaz et al. 2009; Goerdt et al. 2010) does not appear to play a dominant role in our simulations. In the LT simulations, no cores form; therefore effects of dynamical friction are ruled out except from the densest clumps in HT. In the HT simulations, any dense infalling clumps are typically disrupted long before they reach the inner kiloparsec. To test the effect of dynamical friction, one would first need to remove the explosive events associated with feedback. However as the feedback energy is decreased, dense clumps start to pile up in galaxies until time integration becomes computationally unfeasible, at the same time creating an unrealistic dense central bulge. Additionally we do not have the resolution to produce star clusters (Goerdt et al. 2010) which could be more robust to disruption than gas clumps. As a result we are not ruling out dynamical friction as an agent for weakening cusps except for the particular simulations in use here.

The DG1 case (which undergoes major mergers at  $z = 3$  and  $z = 1$ ; see Section 2) has a very similar cusp-flattening history to the galaxy described in this work. The mergers themselves have no measurable effect on the halo slope and, as expected through arguments based on Liouville’s theorem, cores remain present after the merger (Kazantzidis et al. 2006). In Governato et al (in prep.) we show that cores form in the large majority of dwarf galaxies, irrespective of their assembly history.

The model is reminiscent of the violent relaxation envisioned by Lynden-Bell (1967), although our analysis does not attempt to generate the gravitational potential self-consistently. It would thus be desirable in the future to work the microphysics into a broader, analytical description of the evolution of a self-consistent dark matter distribution function. We would further like to investigate the importance of departures from exact spherical symmetry. The simulated supernova explosions are rarely exactly on the axis of the disk, so even axisymmetry is violated. This will lead to the non-conservation of angular momentum, which must be understood before we can investigate the impact of the process on the anisotropy of the orbits (Tonini et al. 2006).

Stars, like dark matter particles, are collisionless and therefore should be subject to the same migratory processes outlined here. Stars forming near the centre of the HT galaxies indeed migrate outwards; it could be natural in this context that the scale-length of the dark matter cores and the stellar disks are approximately equal, an observational relation noted by Gentile et al. (2009). Indeed the scale-lengths of both stellar disk and dark matter core of the dwarf galaxies discussed here are approximately 1 kpc (G10; Brooks et al. 2011). To make this link convincing will require a more systematic study of scaling with mass (Brooks et al in prep.).

While the analytic model we have described is independent of

the detailed gas dynamics, to obtain results the simulated hydrodynamics are used as an input. The cusp-flattening effect is therefore only achieved in reality if the rapid gas motions predicted by the SPH code are reproduced. Mesh-based codes (Teyssier 2002; O’Shea et al. 2004; Springel 2010) highlight potential shortcomings of traditional SPH such as its poor handling of instabilities related to sharp density contrasts (Agertz et al. 2007; Bauer & Springel 2011). In future we intend to address the sensitivity of our results to these inaccuracies through comparison with alternative codes and use of forthcoming improvements to the *Gasoline* SPH engine that reduce artificial surface tension (see also Read & Hayfield 2011). Through direct comparison of various codes Scannapieco et al. (2011) conclude that, for most practical purposes, the choice of sub-grid model approximation (via which supernova energy is coupled to the gas) is more critical than the numerical technique. It will be of interest to determine whether other feedback mechanisms and numerical methods can reproduce our results. Indeed recently Martizzi et al. (2011) reported the formation of dark matter cores in AMR simulations through gas fluctuations very similar to ours, but driven by AGN activity in clusters.

We are currently investigating how the cores scale for  $10^9 M_\odot < M_{\text{vir}} < 10^{12} M_\odot$  (Governato et al. in prep). At higher masses the results will depend on a detailed interplay between the deepening dark matter potential, increased star formation rates, and the nature of AGN feedback (Martizzi et al. 2011). The challenge of running suitable simulations to tackle the most massive systems at sufficient resolution is formidable, but one that we hope to tackle in due course.

## ACKNOWLEDGEMENTS

We thank the anonymous referee for helpful comments. AP thanks Steven Gratton for many helpful discussions and James Wadsley, Justin Read, Jorge Peñarrubia, Alyson Brooks, Fergus Simpson, Hiranya Peiris, Gary Mamon and Max Pettini for comments on a draft version of the paper. FG acknowledges support from a NSF grant AST-0607819 and NASA ATP NNX08AG84G.

The analysis was performed using the pynbody package (<http://code.google.com/p/pynbody>). Simulations and analysis were performed using the Darwin Supercomputer of the University of Cambridge High Performance Computing Service (<http://www.hpc.cam.ac.uk>), provided by Dell Inc. using Strategic Research Infrastructure Funding from the Higher Education Funding Council for England.

## References

Agertz, O., et al. 2007, MNRAS, 380, 963  
 Bauer, A., & Springel, V. 2011, MNRAS, submitted, arXiv:1109.4413  
 Bigiel, F., Leroy, A., Walter, F., Brinks, E., de Blok, W. J. G., Madore, B., & Thornley, M. D. 2008, AJ, 136, 2846  
 Binney, J., Gerhard, O., & Silk, J. 2001, MNRAS, 321, 471  
 Binney, J., & Tremaine, S. 1987, Galactic dynamics (Princeton, NJ, Princeton University Press, 1987, 747 p.)  
 Brook, C. B., et al. 2011, MNRAS, 415, 1051  
 Brooks, A. M., et al. 2011, ApJ, 728, 51

Bullock, J. S., Dekel, A., Kolatt, T. S., Kravtsov, A. V., Klypin, A. A., Porciani, C., & Primack, J. R. 2001, ApJ, 555, 240  
 Ceverino, D., & Klypin, A. 2009, ApJ, 695, 292  
 Cole, D. R., Dehnen, W., & Wilkinson, M. I. 2011, MNRAS, 416, 1118  
 Dubinski, J., & Carlberg, R. G. 1991, ApJ, 378, 496  
 Dutton, A. A. 2009, MNRAS, 396, 121  
 El-Zant, A., Shlosman, I., & Hoffman, Y. 2001, ApJ, 560, 636  
 Flores, R. A., & Primack, J. R. 1994, ApJ, 427, L1  
 Gelato, S., & Sommer-Larsen, J. 1999, MNRAS, 303, 321  
 Gentile, G., Famaey, B., Zhao, H., & Salucci, P. 2009, Nature, 461, 627  
 Gnedin, O. Y., & Zhao, H. 2002, MNRAS, 333, 299  
 Goerdt, T., Moore, B., Read, J. I., & Stadel, J. 2010, ApJ, 725, 1707  
 Goldstein, H., Poole, C., & Safko, J. 2002, Classical Mechanics, 3rd edition (Addison Wesley)  
 Governato, F., et al. 2010, Nature, 463, 203  
 Katz, N., Weinberg, D. H., & Hernquist, L. 1996, ApJS, 105, 19  
 Katz, N., & White, S. D. M. 1993, ApJ, 412, 455  
 Kazantzidis, S., Zentner, A. R., & Kravtsov, A. V. 2006, ApJ, 641, 647  
 Kennicutt, Jr., R. C., et al. 2007, ApJ, 671, 333  
 Lynden-Bell, D. 1967, MNRAS, 136, 101  
 Martizzi, D., Teyssier, R., Moore, B., & Wentz, T. 2011, MNRAS, submitted, arXiv:1112.2752  
 Mashchenko, S., Couchman, H. M. P., & Wadsley, J. 2006, Nature, 442, 539  
 Mashchenko, S., Wadsley, J., & Couchman, H. M. P. 2008, Science, 319, 174  
 McGaugh, S. S., Schombert, J. M., de Blok, W. J. G., & Zagursky, M. J. 2010, ApJ, 708, L14  
 Mo, H. J., & Mao, S. 2004, MNRAS, 353, 829  
 Moore, B. 1994, Nature, 370, 629  
 Navarro, J. F., Eke, V. R., & Frenk, C. S. 1996a, MNRAS, 283, L72  
 Navarro, J. F., Frenk, C. S., & White, S. D. M. 1996b, ApJ, 462, 563  
 Navarro, J. F., & White, S. D. M. 1993, MNRAS, 265, 271  
 Oh, S., Brook, C., Governato, F., Brinks, E., Mayer, L., de Blok, W. J. G., Brooks, A., & Walter, F. 2011a, AJ, 142, 24  
 Oh, S.-H., de Blok, W. J. G., Brinks, E., Walter, F., & Kennicutt, Jr., R. C. 2011b, AJ, 141, 193  
 O’Shea, B. W., Bryan, G., Bordner, J., Norman, M. L., Abel, T., Harkness, R., & Kritsuk, A. 2004, in Adaptive Mesh Refinement – Theory and Applications, ed. T. Plewa, T. Linde, & V. Weirs (Springer Lecture Notes in Computational Science and Engineering)  
 Pasetto, S., Grebel, E. K., Berczik, P., Spurzem, R., & Dehnen, W. 2010, A&A, 514, A47+  
 Read, J. I., & Gilmore, G. 2005, MNRAS, 356, 107  
 Read, J. I., & Hayfield, T. 2011, MNRAS, submitted, arXiv:1111.6985  
 Romano-Díaz, E., Shlosman, I., Heller, C., & Hoffman, Y. 2009, ApJ, 702, 1250  
 Romano-Díaz, E., Shlosman, I., Hoffman, Y., & Heller, C. 2008, ApJ, 685, L105  
 Saitoh, T. R., Daisaka, H., Kokubo, E., Makino, J., Okamoto, T., Tomisaka, K., Wada, K., & Yoshida, N. 2008, PASJ, 60, 667  
 Scannapieco, C., et al. 2011, MNRAS submitted, arXiv:1112.0315  
 Shen, S., Wadsley, J., & Stinson, G. 2010, MNRAS, 407, 1581



- Simon, J. D., Bolatto, A. D., Leroy, A., Blitz, L., & Gates, E. L. 2005, *ApJ*, 621, 757
- Springel, V. 2010, *MNRAS*, 401, 791
- Stinson, G., Seth, A., Katz, N., Wadsley, J., Governato, F., & Quinn, T. 2006, *MNRAS*, 373, 1074
- Tacconi, L. J., et al. 2010, *Nature*, 463, 781
- Teyssier, R. 2002, *A&A*, 385, 337
- Tonini, C., Lapi, A., & Salucci, P. 2006, *ApJ*, 649, 591
- van den Bosch, F. C., Burkert, A., & Swaters, R. A. 2001, *MNRAS*, 326, 1205
- Wadsley, J. W., Stadel, J., & Quinn, T. 2004, *New Astronomy*, 9, 137
- Weinberg, M. D., & Katz, N. 2002, *ApJ*, 580, 627